conclude that 1) time and spatial dependent variables in the two-phase impingement equation are separable; 2) our results agree well with method of characteristics solutions for gas expansion in a vacuum when the analytical model for 100% quality is used; and 3) it is important to consider the re-emission momentum exchange at the impingement surface for both the gas and solid phases; it is the same order of magnitude as the impact momentum.

References

[1] Walburn, A. B., "An Analytical and Experimental Examination of the Effect of Cryogenic Propellant Venting on Orbital Vehicle Dynamic Behavior," American Astronautical Society Southeastern Symposium in Missiles and Aerospace Vehicles Sciences, Dec. 1966.

[2] Schlichting, H., *Boundary Layer Theory*, McGraw-Hill, New York, 1960.

[3] Lipemann, H. W. and Roshko, A., *Elements of Gas Dynamics*, Wiley, New York, 1957.

[4] Hayes, W. D. and Probstein, R. F., *Hypersonic Flow Theory*, Academic Press, New York, 1959.

Re-Entry Dispersions Due to Atmospheric Uncertainties

GERALD R. WEISS*
IBM Federal Systems Division West, Westlake Village, Calif.

Nomenclature

A	=	reference area
c	=	sensitivity coefficient
C_D	=	drag coefficient
d	=	correlation distance
$E\{\ \}$	=	expected value operator
g	=	gravitational acceleration
g_c	=	mass-weight conversion factor
h	=	altitude
$\mathbf{P}$	=	covariance matrix
r	=	correlation coefficient
R	=	autocorrelation function
S	=	trajectory arc length
ΔS	=	arc length error
t	=	time
V	=	velocity
ΔV	=	velocity error
ω	=	white noise random variable
W	=	weight
ρ	=	density
$\Delta\rho$	=	density error
β	=	ballistic coefficient $- W/C_DA$
γ	=	flight-path angle referenced to local horizontal
σ^2	=	variance

Subscripts

i	=	ith atmosphere layer
0	=	initial conditions
s	=	arc length
x	=	downrange coordinate
y	=	vertical coordinate

Introduction

AN important factor in the evaluation of re-entry vehicle performance is the determination of trajectory dispersions due to geophysical environmental errors. For re-entry trajectories, a principal environmental error source is local variations in the atmospheric density. Present analytical techniques for determining atmospheric induced trajectory dispersions include the Sissenwine[1] density covariance method and the Purcell-Barbery[2] temperature covariance method. The fundamental equation used in both methods is

$$\sigma_s^2 = \sum_i \sum_j c_i c_j r_{ij} \sigma_i \sigma_j \tag{1}$$

where r_{ij} are the density correlation coefficients between ith and jth atmosphere layers in the density covariance method, and the temperature correlation coefficients between atmosphere layers in the temperature covariance method. Both methods require perturbation of the model atmosphere's discrete parameters to determine the influence coefficients c_i. The correlation coefficients are obtained by statistical reduction of meteorological data. The technique produces the covariance in the trajectory state at the specific altitude at which the influence coefficients are evaluated.

The purpose of this Note is to present an alternate technique for determining trajectory dispersions due to atmospheric uncertainties. The technique is termed the atmospheric random process method (ARP) because it assumes that the trajectory error state equations are forced by an atmosphere whose parameters are described by an exponentially correlated random process. The ARP technique results in a set of continuous differential equations for the variances of the trajectory state, the solution of which yields a continuous altitude history of the dispersion growth. The method is illustrated for the scalar trajectory variable, arc length, and the scalar atmospheric error source, density.

Atmospheric Density Model

The true density of the atmosphere at any altitude above the earth's surface is modelled as a mean value plus an additive noise term,

$$\rho_{\text{true}} = \rho_{\text{mean}} + \Delta\rho_{\text{noise}} \tag{2}$$

The autocorrelation function for the noise density is assumed to be

$$R(h,h + \Delta h) = E\{\Delta\rho(h)\Delta\rho(h + \Delta h)\} = \sigma^2(h)e^{-|\Delta h|/d} \tag{3}$$

where $\sigma(h)$ = standard deviation of the noise density, d = correlation distance of the noise density, and Δh = difference between any two altitudes.

Examination of statistically reduced meteorological data[1] for St. Paul Island, Alaska and Omaha, Nebraska for various seasons of the year reveals that, typically, the noise density standard deviation is not stationary with respect to altitude. Its value is, however, nearly proportional to the local mean density. The simulation results presented in this Note, thus, are based on a standard deviation given by

$$\sigma(h) = K\rho(h) \tag{4}$$

where K is varied between 1% and 5%. If the standard deviation of a specific local density profile is known, Eq. (4) may be replaced by a tabular value set during simulation.

Analysis

The perturbation equations for re-entry arc length are given by

$$d(\Delta S)/dt = \Delta V \tag{5}$$

$$d(\Delta V)/dt = (g_cV^2/2\beta)\Delta\rho \tag{6}$$

Changing the independent variable from time to altitude, the perturbation equations become

$$d(\Delta S)/dy = \Delta V/V \sin\gamma \tag{7}$$

$$d(\Delta V)/dy = (g_cV/2\beta \sin\gamma)\Delta\rho \tag{8}$$

$$d(\Delta\rho)/dy = -\Delta\rho/d + \omega(y) \tag{9}$$

Received May 19, 1969; revision received July 11, 1969.

* Staff Engineer, Guidance Software Department. Associate Member AIAA.

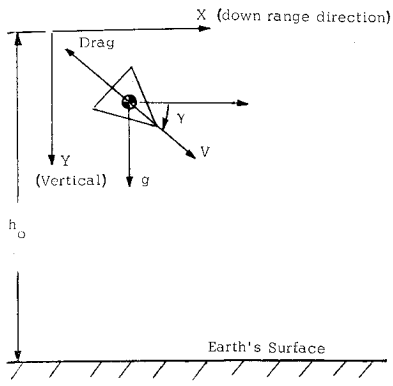

Fig. 1 Re-entry geometry.

Equation (9) is a linear "shaping" filter forced by white noise[3] and produces a noise density that has an autocorrelation function given by Eq. (3).

The differential equation describing the propagation of the covariance matrix of (7) through (9) is given by the Riccati equation,[3]

$$\mathbf{P}' = \mathbf{FP} + \mathbf{PF}^T + \mathbf{GQG}^T \tag{10}$$

where $'$ denotes differentiation with respect to altitude and $\mathbf{P}$ the state covariance is defined as

$$P = E\{[\Delta S \Delta V \Delta \rho]^T [\Delta S \Delta V \Delta \rho]\} \tag{11}$$

The matrices $\mathbf{F}$, $\mathbf{G}$, and $\mathbf{Q}$ are given by

$$\mathbf{F} = \begin{bmatrix} 0 & f_s & 0 \\ 0 & 0 & f_V \\ 0 & 0 & -1/d \end{bmatrix} \tag{12}$$

where

$$f_s = 1/V \sin\gamma \tag{13}$$

$$f_V = g_c V/2\beta \sin\gamma, \ \mathbf{G} = \text{identity matrix} \tag{14}$$

and

$$\mathbf{Q} = \begin{bmatrix} 0 & 0 & 0 \\ 0 & 0 & 0 \\ 0 & 0 & 2\sigma^2(h)/d \end{bmatrix} \tag{15}$$

Since the covariance matrix is symmetric, the 9 element matrix equation (10) reduces to the following 6 first-order equations:

$$\mathbf{P}'_{11} = 2f_s \mathbf{P}_{12} \tag{16}$$

$$\mathbf{P}'_{12} = f_s \mathbf{P}_{22} + f_V \mathbf{P}_{13} \tag{17}$$

$$\mathbf{P}'_{13} = -\mathbf{P}_{13}/d + f_s \mathbf{P}_{23} \tag{18}$$

$$\mathbf{P}'_{22} = 2f_V \mathbf{P}_{23} \tag{19}$$

$$\mathbf{P}'_{23} = -\mathbf{P}_{23}/d + f_V \mathbf{P}_{33} \tag{20}$$

$$\mathbf{P}'_{33} = -2\mathbf{P}_{33}/d + 2\sigma^2(h)/d \tag{21}$$

with initial conditions

$$\mathbf{P}_{11(h_0)} = \mathbf{P}_{12(h_0)} = \mathbf{P}_{13(h_0)} = \mathbf{P}_{22(h_0)} = \mathbf{P}_{23(h_0)} = 0$$

$$\mathbf{P}_{33(h_0)} = \sigma^2(h_0) \tag{22}$$

Simulation Results

Equations (16–21) were solved numerically for several typical re-entry trajectories and noise density parameters. The following trajectory state equations, based on the flat, nonrotating earth model illustrated in Fig. 1, were used to provide the nominal trajectory state:

$$x' = V_x/V_y \tag{23}$$

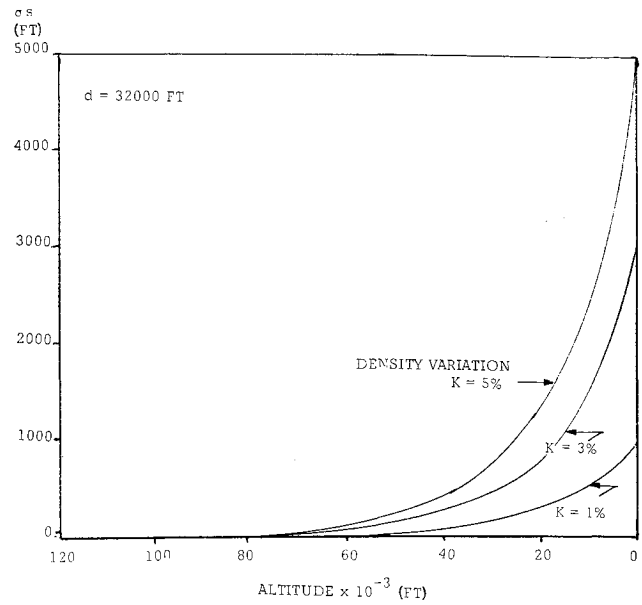

Fig. 2 Arc standard deviation altitude history.

$$V'_x = (-g_c \rho V/2\beta) V_x/V_y \tag{24}$$

$$V'_y = -g_c \rho V/2\beta + g/V_y \tag{25}$$

$$t' = 1/V_y \tag{26}$$

$$V = (V_x^2 + V_y^2)^{1/2} \tag{27}$$

The 1962 U.S. Standard Atmosphere[4] was used to provide the mean density values.

Figure 2 illustrates the growth of the arc length standard deviation $(\mathbf{P}_{11})^{1/2}$ with decreasing altitude. The predominant growth in the lower atmosphere is due to the rapidly increasing density forcing function and the rapidly decreasing velocity. The velocity effect is illustrated by Eqs. (13) and (16) which show that the rate of change of the arc length dispersion varies with the inverse of the velocity. Because of the velocity sensitivity, closed-form solutions[5] for the trajectory velocity (which neglect gravity) were found to be inadequate at the lower altitudes and numerical integration of of Eqs. (23–27) was required.

Simulation results show that the arc length dispersion (σ_s) is linearly related to the noise density uncertainty (K). The resultant linearity is due to the linear relationship between arc length error and density error and the assumed proportionality between the noise density standard deviation and the mean density.

Concluding Remarks

The ARP technique provides a method for generation of trajectory dispersions due to atmospheric error sources that can be modelled as exponentially correlated random processes. In addition, if the noise sources are assumed to be Gaussian distributed, probabilistic statements such as the re-entry trajectory CEP (circular error probable) can be made.

Since the ARP method does not require perturbation runs to determine influence coefficients, significant savings in computational burden can be expected in comparison with the covariance methods. Such savings are especially important during preliminary design phases where vehicle, trajectory, and atmospheric parameters are not precisely defined.

References

[1] Valley, S., ed., *Handbook of Geophysics and Space Environments*, McGraw-Hill, New York, 1965, Chap. 3.

[2] Purcell, W. E. and Barbery, T. B., "Dispersions Resulting

from Atmospheric Variations," *Journal of Spacecraft and Rockets*, Vol. 5, No. 8, Aug. 1968. pp. 1005–1007.

[3] Bryson, A. E., Jr. and Ho, Y.-C., "Applied Optimal Control," *AIAA Professional Study Series*, AIAA, New York, Aug. 1967, Chap. 11.

[4] *U.S. Standard Atmosphere*, U.S. Government Printing Office, Dec. 1962.

[5] Allen, H. J. and Eggers, A. J., Jr., "A Study of the Motion and Aerodynamic Heating of Ballistic Missiles Entering the Earth's Atmosphere at High Supersonic Speeds," Rept. 1381, 1958, NACA.

Re-Entry Vehicle Roll Control Utilizing Recirculating Base Flow

M. D. Bennett* and Amado A. Trujillo†
Sandia Laboratories, Albuquerque, N.Mex.

Nomenclature

A = vehicle base area
C_l = rolling moment coefficient, $L/q_\infty Ad$
$C_{N\theta}$ = vehicle normal force coefficient per unit angle of attack, $\partial C_N/\partial\theta$
d = vehicle base diameter
I_x = mass moment of inertia about vehicle longitudinal axis
I_y = mass moment of inertia about vehicle lateral axis
q_∞ = freestream dynamic pressure
S = fin planform area
$x_{c.p.}$ = distance from vehicle's center of mass to center of pressure
y = lateral distance from vehicle's center of mass to axis of aerodynamic symmetry
α_t = nonrolling vehicle trim angle of attack
θ = vehicle resultant angle of attack
$(\dot{})$ = denotes differentiation with respect to time

Introduction

Ballistic bodies with small asymmetries about the spin axis may exhibit erratic behavior when the roll and nutational frequencies are approximately equal.[1–4] The roll resonance phenomenon may not pose a serious design problem for a re-entry vehicle of large size because the rotational asymmetries are relatively minor. However, because of the inequality of scaling laws for mass and aerodynamic properties, and the possibility of proportionally more asymmetric ablation of the heatshield or significant thermal distortion of the body, the susceptibility to roll resonance increases as the geometric size of the vehicle decreases or as the ballistic factor increases.[5–8] Control of the vehicle roll position, or its space or time derivatives, is required when it is impractical to restrict the configurational asymmetry enough to prevent persistent roll resonance.

The novel roll-control concept discussed in this Note consists of a number of blades or fins that are attached to the base of the vehicle (Fig. 1) and are oriented such that their reaction to the small, but not insignificant, radial component of the flow along the cone base produces a rolling moment. This control system has several attractive features. The low heat-transfer rates in the region of the fins provide a distinct and important design advantage over systems using conventional, exposed aerodynamic surfaces. Lockman[9] shows that the heat-transfer rate at the center of the base is about two orders of magnitude less than at the nose stagnation point.

Received June 2, 1969; revision received July 31, 1969. This work was supported by U.S. Atomic Energy Commission.

* Staff Member, Aeroballistics Division. Associate Fellow AIAA.

† Staff Member, Experimental Aerodynamics Division. Member AIAA.

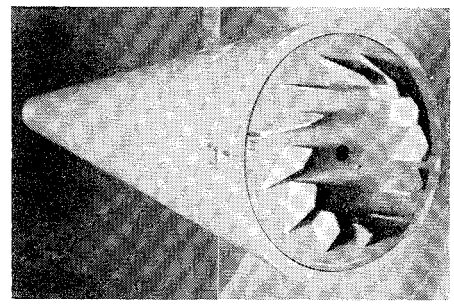

Fig. 1 Re-entry vehicle model in hypersonic wind tunnel showing cone-support strut and base impeller.

Unlike systems that employ control jets, an onboard gas system is not required. The major disadvantage of the system is the limited torque available for the control function.

Wind-Tunnel Tests

Three base impeller configurations were evaluated at zero angle of attack, Mach 7.3, and at a freestream Reynolds number of 0.55×10^6 based on cone base diameter. The model was supported in the test section by a slender, transverse strut to minimize the flow interference effects in the recirculation zone. A portion of the strut can be seen in Fig. 1. The model was a 10° half-angle cone having a 4-in. base diameter and a 0.375-in. nose radius. The boundary-layer flow at the cone base was laminar.

The three impeller configurations are shown in Fig. 2. Configurations A and B each contain 12 fins that have a combined planform area of 2.50 and 3.58-in., respectively; configuration C has 8 fins with a combined area of 5.60-in. The fin span of all three configurations was maintained constant at 0.60-in. or 15% of the cone base diameter.

During tests, the impeller was attached to a shaft mounted on ball bearings located inside the conical model so that the fin assembly could rotate relative to the stationary body. The assembly was locked in position until steady-state flow conditions in the wind tunnel were achieved; then it was remotely released. The rolling moment was calculated from measurements of the angular acceleration of the impeller and the mass moment of inertia of the rotating components. The results were corrected for bearing friction, which amounted to approximately 15% of the maximum aerodynamic driving moment. The bearing friction was determined before each data run by measuring the angular deceleration of the impeller in a vacuum environment.

As may be seen in Figs. 1 and 2, the trailing (outer) edges of the fins are swept forward with respect to the cone axis; the amount of the sweep is 30° measured from a normal to the plane of the cone base. In the initial tests, both the leading and trailing edges were perpendicular to the plane of the cone base, and all three impeller configurations either failed to rotate or rotated opposite to the anticipated direction. Apparently a part of the forebody boundary-layer flow, expanding around the corner of the cone base and entering the recirculation zone, was impinging upon the trailing portion of the

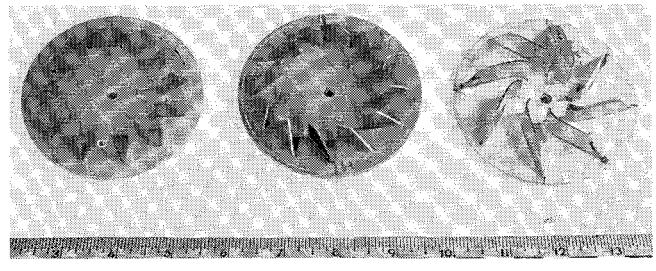

Fig. 2 Experimental base impeller configurations (from left to right, configurations A, B, and C).